PROTEINS: Structure, Function, and Genetics 41:374–384 (2000)

A Comparative Structural Analysis of the ADF/Cofilin Family

Gregory D. Bowman,[1,2] Ilana M. Nodelman,[1,2] Yan Hong,[3] Nam-Hai Chua,[4] Uno Lindberg,[5] and Clarence E. Schutt[2]*

[1]*Department of Molecular Biology, Lewis Thomas Laboratories, Princeton University, Princeton, New Jersey*
[2]*Department of Chemistry, Henry H. Hoyt Laboratory, Princeton University, Princeton, New Jersey*
[3]*Laboratory of Plant and Cell Biology, Institute of Molecular Agrobiology, National University of Singapore, Science Park, Singapore*
[4]*Laboratory of Plant Molecular Biology, The Rockefeller University, New York, New York*
[5]*Department of Zoological Cell Biology, WGI, Arrhenius Laboratories for Natural Sciences, Stockholm University, Stockholm, Sweden*

ABSTRACT **Actin-depolymerizing factor (ADF) and cofilin define a family of actin-binding proteins essential for the rapid turnover of filamentous actin in vivo. Here we present the 2.0 Å crystal structure of *Arabidopsis thaliana* ADF1 (AtADF1), the first plant crystal structure from the ADF/cofilin (AC) family. Superposition of the four AC isoform structures permits an accurate sequence alignment that differs from previously reported data for the location of vertebrate-specific inserts and reveals a contiguous, vertebrate-specific surface opposite the putative actin-binding surface. Extending the structure-based sequence alignment to include 30 additional isoforms indicates three major groups: vertebrates, plants, and "other eukaryotes." Within these groups, several structurally conserved residues that are not conserved throughout the entire AC family have been identified. Residues that are highly conserved among all isoforms tend to cluster around the tryptophan at position 90 and a structurally conserved kink in α-helix 3. Analysis of surface character shows the presence of a hydrophobic patch and a highly conserved acidic cluster, both of which include several residues previously implicated in actin binding. Proteins 2000;41:374–384.**

Key words: actin-depolymerizing factor; crystal structure; cytoskeleton; isoform; proteomics

INTRODUCTION

Orchestrated networks of actin filaments and associated proteins comprise the eukaryotic microfilament (MF) system, an organization essential for many basic cellular processes. As exemplified by the dynamic nature of membrane ruffling,[1] exocytosis,[2] and cytokinesis,[3] an important characteristic of the MF system is its ability to be rapidly remodeled according to intra- and extracellular cues. Actin-depolymerizing factor (ADF) and cofilin define a family of small, monomeric proteins that bind to monomeric (G) and filamentous (F) actin and increase the rate of filament polymerization and depolymerization.[4,5] This activity has been shown in vitro, for example, using the intracellular bacterial pathogen *Listeria monocytogenes*, where depletion of ADF/cofilin (AC) slows bacterial motility and lengthens the F-actin comet tails.[6,7] In studies of cofilin mutants in *Saccharomyces cerevisiae*, wild-type AC activity is necessary for rapid depolymerization of yeast actin cortical patches, suggesting that AC family members are the primary agents responsible for the rapidity of actin turnover in vivo.[8] Disruption of AC isoforms in *S. cerevisiae*,[9,10] *Caenorhabditis elegans*,[11] and *Drosophila melanogaster*[12] is lethal, highlighting the critical role of AC proteins in maintaining the plasticity of the MF system.

ADF, cofilin, depactin, and actophorin were first identified in chick,[13] pig,[14] starfish,[15] and amoeba[16] as actin-binding proteins that rapidly depolymerize filamentous actin in vitro and were eventually shown to increase the rate of F-actin polymerization as well. The apparent paradox of stimulating both actin polymerization and depolymerization has been explained as a severing activity. Since the AC proteins do not cap actin filament ends as in the case of gelsolin proteins, the creation of more plus (barbed) and minus (pointed) ends of F-actin via severing would presumably allow for faster F-actin turnover.[14,17,18] Carlier and coworkers,[7,19] however, have instead proposed that the mechanism of AC action involves acceleration of the treadmilling cycle by increasing the rate of pointed-end dissociation. Although a combination of severing and increased treadmilling has also been suggested,[20–22] several recent reports find that a severing mechanism is sufficient to account for AC activity.[23–25]

The AC family is regulated by phosphorylation, phosphoinositide binding, pH, the state of the actin-bound nucleotide, and nuclear translocation. Inhibitory phosphorylation of AC proteins by LIM kinase[26,27] targets a conserved

Grant sponsor: Swedish Natural Science Council; Grant sponsor: Swedish Cancer Foundation; Grant Sponsor: National Science and Technology Board, Singapore; Grant Sponsor: National Institutes of Health.

*Correspondence to: Clarence E. Schutt, Department of Chemistry, Henry H. Hoyt Laboratory, Princeton University, Princeton, NJ 08544. E-mail:schutt@chemvax.princeton.edu

Received 24 April 2000; Accepted 14 July 2000

N-terminal serine.[28,29] Like the other AC crystal structures,[30,31] the structure of N-terminally phosphorylated actophorin from *Acanthamoeba castellanii* does not reveal the positioning for the phosphorylated serine residue due to disorder.[32] The absence of a stable intramolecular interaction involving the phosphoserine suggests that phosphorylation blocks AC activity by directly altering the character of the actin-binding surface. In contrast, phosphoinositides have been shown to block the AC:actin interaction through competition. A cofilin-derived dodecamer peptide that binds weakly but specifically to phosphoinositides contains two actin-interacting basic residues on the loop preceding α-helix 3, suggesting that phosphoinositides and actin recognize overlapping sites.[33] The activity of several AC isoforms is also sensitive to pH, with elevated pH levels resulting in increased depolymerization.[34,35] Signaling events, such as integrin binding[36,37] and growth factor stimulation,[38,39] result in a local increase in pH and mobilization of the actin cytoskeleton, suggesting a possible in vivo regulatory role for this pH-dependent depolymerization activity.[4] The state of the actin-bound nucleotide is also a determining factor in AC binding and activity as seen from the increased affinity for ADP-actin compared with ATP-actin.[7,23,40,41] Another manner in which cells might regulate AC activity includes nuclear translocation upon various cellular stresses.[42] The presence of a putative nuclear localization signal (NLS) sequence in vertebrate AC proteins is believed to be responsible for the formation of nuclear cofilin:actin "rods"[42], however it remains to be determined if this sequence is necessary for the translocation.

Although the atomic details of the AC:actin interaction are not known, mutagenesis, high-resolution structure determination, and cryoelectron microscopy have provided insight into the AC:actin complex. Extensive mutagenesis data have accumulated from work with porcine,[21,43] yeast,[44] maize,[45] and *C. elegans*[46] isoforms regarding residues that do and do not disrupt actin binding to varying degrees. Placement of actin-interacting residues into a structural context has been possible with the structure determinations of human destrin (also known as ADF1),[47] *S. cerevisiae* cofilin,[30] and *Acanthamoeba* actophorin.[31,32] The AC-fold is built from a central, mixed β-sheet flanked by two α-helices on each face. The putative actin-binding site includes the N-terminus and residues located on and preceding helices 3 and 4, which primarily map to the edge and part of one face of the disk-shaped molecule (for review see Lappalainen et al[48] and Bamburg et al[49]). Cryoelectron microscopic studies of the AC:actin interaction have offered a more global and functionally revealing view. McGough and coworkers have shown AC binding to filamentous actin induces a 5° twist, suggesting a structural mechanism for AC-induced depolymerization. [49,50]

Here we report the crystal structure of *Arabidopsis thaliana* actin-depolymerizing factor 1 (AtADF1), the first AC structure from the plant kingdom. By using available sequence and structural data, an overall comparative analysis of the AC family was performed. Notably, two major insertions and a C-terminal extension of the vertebrate isoforms form an extensive and contiguous surface not present in other family members. Many highly conserved amino acid positions cluster together in the structure and form networks of interactions that are maintained throughout these AC isoform structures. In addition, a comparative analysis underscores regions on the surface of the AC isoforms that are conserved in character and shows that the putative actin-binding face has remained more conserved than other regions of the surface.

TABLE I. Crystal Parameters and Data Collection Statistics

Space group	$C222_1$
	a = 55.92
	b = 71.35
	c = 63.75
Resolution (Å)	26–2.0
Total reflections	60228
Unique reflections	8926
Completeness (%)	99.1 (99.0)*
I/σ	15.6
R_{merge} (%)[1]	4.5 (13.5)*
Refinement statistics	
Resolution (Å)	26–2.0
R_{work} (%)[2]	21.1
R_{free} (%)[3]	24.4
No. of atoms	1087
B-factor (Å^2)	
Mainchain	28.1
Sidechain	31.1
Water	44.0
LDAO	43.8
r.m.s.‡ deviations from ideality	
Bond lengths (Å)	0.005
Bond angles (°)	1.2

*Values in parentheses represent the highest resolution shell.
‡root mean square.
[1] $R_{merge} = \Sigma|I - \langle I\rangle|/\Sigma\langle I\rangle$.
[2] $R_{work} = \Sigma||F_o| - |F_c||/\Sigma|F_o|$, where F_o and F_c are the observed and calculated amplitudes, respectively.
[3] R_{free} was calculated as R_{work} and contains 10% of total unique reflections omitted from refinement for cross-validation.

RESULTS AND DISCUSSION

Structural Overview

The crystal structure of AtADF1 was solved to 2.0 Å resolution (Table I). The C-terminal 15 residues were disordered due to the presence of a bound detergent molecule and crystal contacts. Displaying an average sequence identity of 41%, AtADF1 superimposes well with the other nonvertebrate isoform structures (yeast cofilin and *Acanthamoeba* actophorin) with an average r.m.s. deviation of 1.05 Å for all Cα atoms excluding α-helix 4 (Fig. 1). Vertebrates have the same global fold yet diverge from other members of the AC family by one minor and two major insertions and a carboxyl-terminal extension. Cα superposition of the three nonvertebrate structures onto human destrin, excluding vertebrate-specific inserts, yields an average r.m.s. deviation of 2.27 Å.

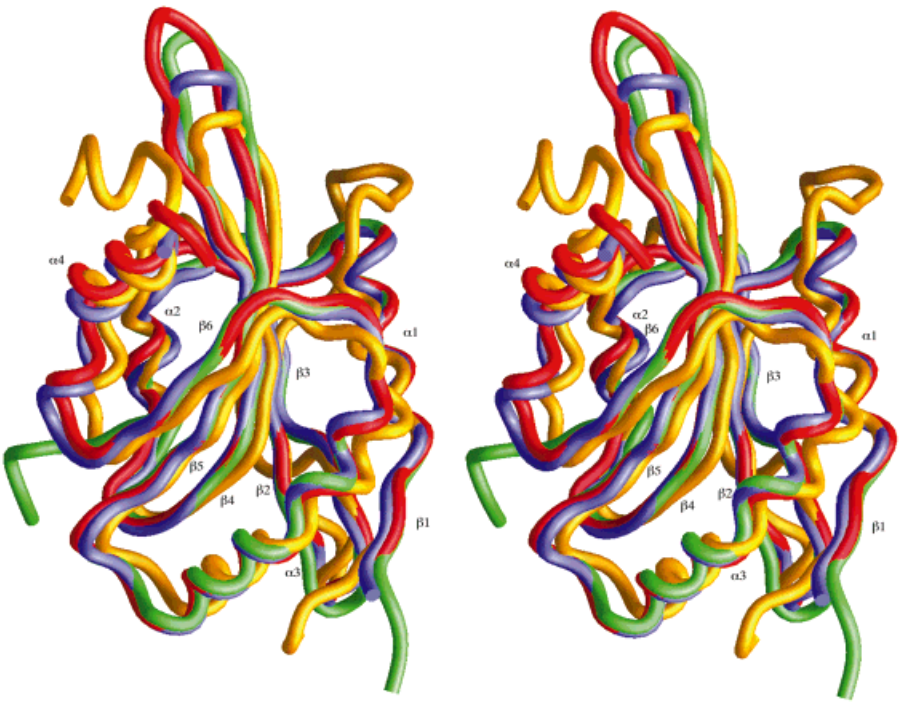

Fig. 1. C_α superposition of AtADF1 (green), *S. cerevisiae* cofilin[30] (red), *Acanthamoeba* actophorin[31] (blue), and human destrin[47] (gold). The final α-helix of AtADF1 is not visible in the crystal structure due to a bound detergent molecule and crystal packing (see Materials and Methods).

Sequence Comparison of the AC Family

Superposition of all ADF/cofilin structures allows for a precise amino acid sequence alignment, including placement of regions with less homology or insertions/deletions relative to the other three sequences. With these structural representatives of the AC family, most of the other 30 AC family members can be readily aligned, with vertebrates, plants, and "other eukaryotes" displaying average sequence identities of approximately 74%, 64%, and 43%, respectively (Fig. 2A,B; the sequence numbering used in the alignment and throughout the text is that of AtADF1 unless otherwise specified). Two relatively divergent isoforms include C. *elegans* unc60A and *Asterias amurensis* (starfish) depactin. The *C. elegans* isoform cannot be reliably aligned between amino acid positions 44 and 53 because of 14 additional residues compared with other nonvertebrates (five additional residues compared with vertebrates) and relatively low-sequence homology (32% average identity with all family members). The isoform from *A. amurensis*, depactin, although being more similar in length to most family members, also displays relatively low sequence homology overall (29% average identity), indicating that alignment of this sequence may misrepresent various structural elements.

Several recent reviews highlight various similarities and differences of the AC family.[48,49] We disagree with several conclusions reached in these reviews that stem from the alignment of the vertebrate-specific inserts. The structure-based sequence alignment presented here positions the first vertebrate specific insert of nine residues between nonvertebrate amino acid positions 25 and 26, the second major insert of seven residues between positions 51 and 52, and a two residue insert between positions 44 and 45. The misplacement of the second major insert and exclusion of the two amino acid insert in other published sequence alignments appear to have arisen from the coincidental matching of the yeast cofilin sequence (38-EIVVKETS) to the human destrin sequence (54-EILVGDVG) instead of the structurally aligned vertebrate sequence (46-CIIVE[EG]KEI) that includes the two amino acid insert (bracketed residues). In addition, this misplacement also led to the conclusion that position 45 in yeast (AtADF1 position 47) is a conserved residue in all AC family members occupied by either a serine or a glycine.[48] Although this position is in fact conserved as glycine or a small amino acid in nonvertebrates, vertebrates have the bulkier isoleucine at this position. Sequence alignments have proven to be a powerful tool for grouping proteins related in structure and function; however, it is evident that the sequence alignment programs have their limitations and should be used with caution to resolve ambiguities (e.g., proper placement of gaps and inserts). With the increasing efforts toward structural genomics, the availability of structural representatives from divergent isoform sequences will allow for more accurate alignments and, therefore, more meaningful representations of unknown structures.

Vertebrate-Specific Inserts

The most striking aspects of the superposition of the four AC structures are two vertebrate-specific inserts found between α-helix 1:β-strand 2 and β-strand 3:α-helix 2. These two inserts are spatially proximal to a vertebrate-specific C-terminal extension that together define a contiguous "horseshoe-shaped" surface around the loop between β-strands 4 and 5, contributing approximately 1,530 $Å^2$ or

22% of the total solvent accessible surface area of the protein (Fig. 3). Surrounded by and interacting with these inserts, this central loop appears to be more structurally stable than in nonvertebrates: the average r.m.s. deviations for this region of the human destrin NMR ensemble indicate good agreement (<1.0 Å) among the top 20 solutions,[47] whereas the B-factors for these residues are relatively high in the nonvertebrate crystal structures. This vertebrate-specific surface is distinct from the actin-binding surface as evidenced by the spatial separation of actin-interacting residues identified by mutagenesis and from the ability of vertebrate isoforms to rescue a yeast cofilin knockout.[10] In an evolutionary sense, it is not surprising that the additional inserts were restricted to these regions given the pressure to maintain the actin binding surface.

The first vertebrate insert contains a putative NLS that is believed to be responsible for the nuclear translocation of AC upon cellular stresses.[51,52] In the crystal structure of the nuclear import factor karyopherin α complexed to the SV40 T antigen NLS, the extensive hydrophobic and charged interactions maintain the signal peptide in an extended conformation.[53] In human destrin, the putative NLS sequence is located at the C-terminal end of a short helix, which would require that this region undergo a conformational change before binding to a nuclear transport factor. Among the 20 solution structures, it was noted that the residues immediately preceding the NLS displayed the highest r.m.s. deviations, indicating this to be an inherently mobile loop.[47] This region may, therefore, function as a molecular switch to dictate the cellular localization of vertebrate AC proteins: in the absence of cellular stresses, occlusion of this region allows the protein to maintain a cytoplasmic localization, whereas on heat shock, DMSO, and other stresses, exposure of the NLS allows the association of a nuclear transport factor and subsequent shuttling to the nucleus.[47] The contiguous surface presented by the second major insert and C-terminal extension may be important for binding/recognition of a vertebrate-specific factor and subsequent conformational changes surrounding the NLS.

Structural Comparison of the AC Family

A closer inspection of the sequence alignment indicates that particular amino acid positions are conserved within the vertebrate, plant, and "other eukaryotes" groups, yet are nonconserved between these groups. Most of these amino acid positions cluster spatially and appear to serve structural roles similar to their isoform counterparts. In vertebrates, positions 29 and 47 (destrin 35 and 55) are strictly conserved as alanine and isoleucine, respectively, whereas most nonvertebrates have an aromatic residue at position 29 and glycine or small amino acid at position 47. In all isoform structures, residues 29 and 47 are in close van der Waals contact with each other and appear to be important for the positioning of the beginning and ending of β-strands 2 and 3, respectively. Also, the aromatic residue at position 72 in nonvertebrates fills a space occupied by vertebrate Ala72 (destrin Ala87) and a bulky side chain (destrin position 161) on the vertebrate-specific C-terminal extension.

Within the vertebrate class, it is notable that the identity of this C-terminal residue (destrin 161) as phenylalanine or leucine correlates with that of position 53 (destrin 68) as phenylalanine or tyrosine, respectively (see Fig. 2). Packing against one another, these two residues appear to stabilize the C-terminus: residue 53 stacks against aromatics at positions 56 and 70 and, as a tyrosine, can hydrogen bond to the backbone carbonyl of residue 127, whereas destrin 161 packs against the aromatics at position 53 and 74 and hydrophobic side chains at positions 134 and 135. The favorable aromatic:aromatic interactions resulting from a phenylalanine at vertebrate position 161 may serve as an energetic trade-off for the hydrogen-bonding potential of a tyrosine at position 53.

For the 34 AC family members represented in the sequence alignment, 80% sequence identity or greater is observed for 28 amino acid positions. Many of these residues perform structurally conserved roles that appear necessary, directly or indirectly, for maintenance of actin-binding surfaces. Trp90 is a highly conserved residue that interacts with loops containing putative actin-binding residues: the indole ring both participates in a hydrogen bond to the backbone carbonyl of residue 61 and makes van der Waals contacts with Leu60, Pro61, Pro92, and the proline/aromatic at position 126 (Fig. 4A).

Another highly conserved motif of the AC family is the "kink" or disruption of α-helical hydrogen bonding in the middle of α-helix 3 (Fig. 4B). Due to the ϕ/ψ angles for residue 106, the backbone carbonyl and amide groups of 104:108 and 105:109 are >5 Å apart. Notably, in the structures of AtADF1 and the phosphorylated form of actophorin, the backbone carbonyls of residues 104 and 105 and the amide of residue 109 participate in hydrogen bonds to two well-ordered water molecules. Given the conserved backbone positioning of this region, the presence of bound water molecules at these positions may be a general feature across the AC family. In all four structures, stabilization of this region appears to be due in part to two highly conserved tyrosines at positions 67 and 103. Pointed in opposition, these two tyrosines stack against one another, each hydrogen bonding to the backbone of or near the other. Removal of either hydroxyl group via mutagenesis to phenylalanine decreases the affinity for actin, suggesting that this region is relatively sensitive to perturbation.[21,45]

As seen from the sequence alignment in Figure 2, the kink in α-helix 3 is surrounded by the most conserved regions of the protein. In particular, positions 104–106 strictly present small side chains, with alanine preferred at position 104 and serine or threonine at positions 105 and 106. The substitution of larger side chains at these positions or elimination of the Ser106 hydroxyl group significantly weakens actin binding,[21,46] suggesting that this region may directly contact actin. It has been proposed that maintenance of the α-helix 3 kink relies primarily on one[21] or both[30] of the serines at positions 105 and 106; however, these residues do not appear to be performing a

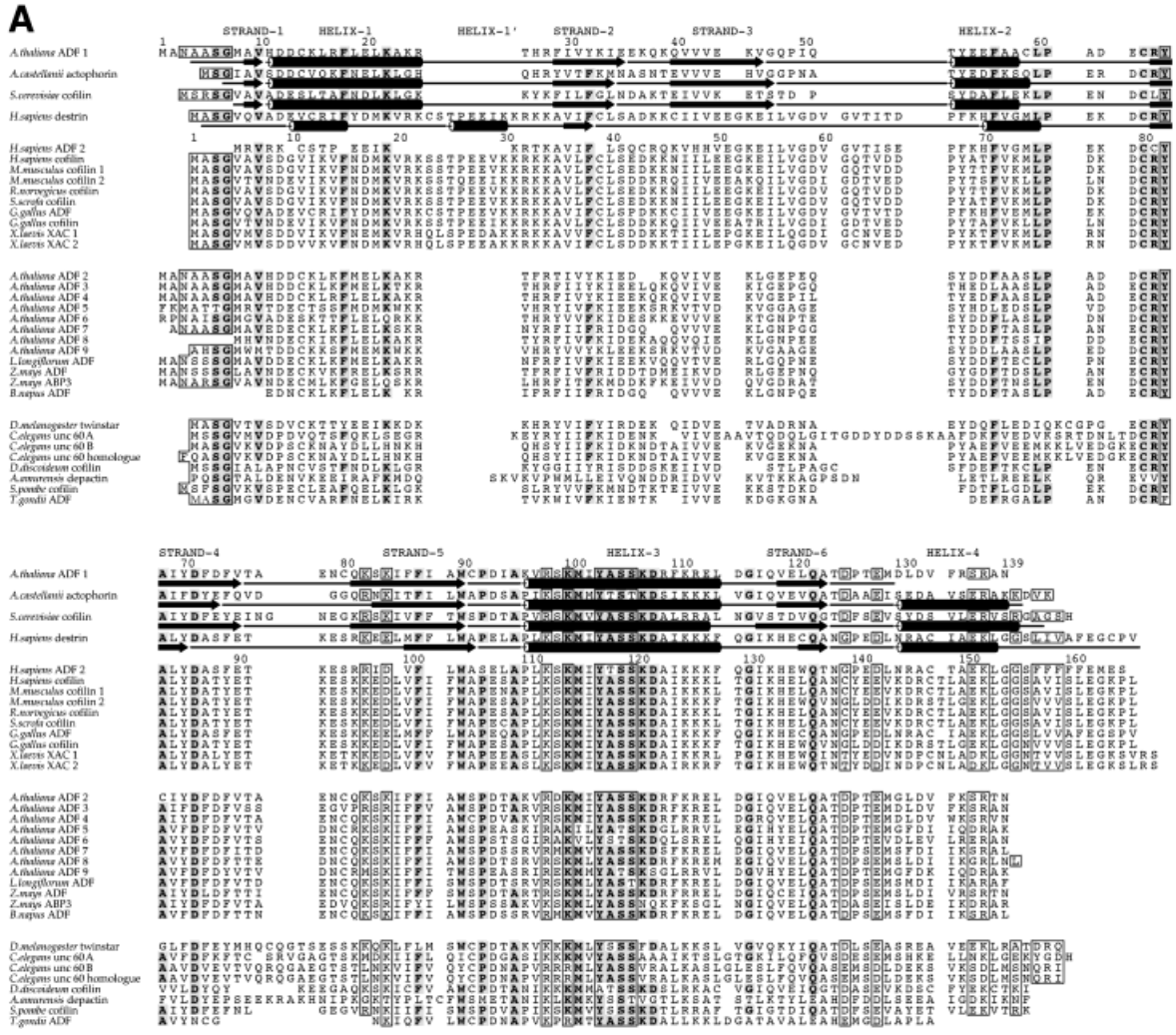

Fig. 2. **A:** Sequence alignment of the AC family. Superposition of AtADF1, *S. cerevisiae* cofilin,[30] *Acanthamoeba* actophorin,[31] and human destrin[47] provided a structure-based alignment. The secondary structure designations (α-helix = cylinder, β-strand = arrow) were calculated by using STRIDE.[63] All other sequences were aligned by using AMPS[64] and ALSCRIPT[65] with modifications based on structural superposition. Below the four structural representatives at the top of the alignment, the remaining 30 AC isoforms are grouped as vertebrates, plants, and "other eukaryotes." Residue numbering at the top of the alignment is that of AtADF1 and is used throughout the text, whereas the numbering above human ADF2 is that of the vertebrate group. Amino acid positions conserved in >78% of AC sequences are shaded in gray. Residues that have been shown by mutagenesis to disrupt actin binding are boxed. **B:** A phylogenetic tree of AC members based on the structure-based sequence alignment. This organization shows the clustering of plant (top) and vertebrate (bottom) sequences, with significantly lower homologies among the more diverse group of "other eukaryotes" (middle). As previously noted, the mammalian and chicken isoforms appear to fall into three categories: muscle cofilin, nonmuscle cofilin, and ADF/destrins.[48] For plants, there is not adequate sequence data to reliably characterize the ADF isoforms into subclasses, yet trends are evident. In *Arabidopsis thaliana,* there is 84% sequence identity among isoforms 1–4, 72% between 7 and 8, and 77% between 5 and 9. AtADF 7 and 8 are more similar to *B. napus* (rapeseed) and *L. longiflorum* (lily) ADF, respectively, than to each other, hinting at divisions similar to those seen in the vertebrate class. The bar represents 10% divergence. This tree was produced by using an initial alignment from Clustal W[66] with appropriately placed sequence gaps for the four structural representatives and graphically displayed with NJPLOT.[67] Sequence ID numbers from GenBank (GB), Swiss Prot (SP), EMBL, and PIR databases are as follows: *Arabidopsis thaliana* ADF 1 (GB:AAC72407); *Acanthamoeba castellanii* actophorin (SP:P37167); *Saccharomyces cerevisiae* cofilin (SP:Q03048); *Homo sapiens* destrin (SP:P18282), ADF2 (GB:U47924), and cofilin (PIR:S12632); *Mus musculus* (mouse) cofilin 1 (PIR:S12584) and 2 (SP:P45591); *Rattus norvegicus* (rat) cofilin (SP:P45592); *Sus scrofa* (pig) cofilin (PIR:A29240); *Gallus gallus* (chick) ADF (PIR:A35702) and cofilin (PIR:B35703); *Xenopus laevis* cofilin 1 (SP:P45695) and 2 (SP:P45593); *A. thaliana* ADF 2 (EMBL:ATF16L2), 3 (GB:AAD09109), 4 (GB:AAD09110), 5 (GB:AAD09113), and 6 (GB:AAF01035); *A. thaliana* ADF 7, 8, and 9 (C-H. Dong and N-H. C., unpublished results); *Lilium longiflorum* (lily) ADF (SP:P30175); *Zea mays* (maize) ADF (SP:P46251) and ABP3 (identical to ADF3, PIR:T02914); *Brassica napus* (rapeseed) ADF (SP:P30174); *Drosophila melanogaster* twinstar (PIR:A57569); *Caenorhabditis elegans* unc60A (SP:Q07750), unc60B (SP:Q07749), and unc60 homolog (PIR:T33952); *Dictyostelium discoideum* cofilin (SP:P54706); *Asterias amurensis* (starfish) depactin (SP:P20690); *Schizosaccharomyces pombe* cofilin (PIR:T38120); and *Toxoplasma gondii* ADF (GB:AAC47717). The first 4, 7, and 21 residues of *A. thaliana* ADF5, ADF6, and *C. elegans* unc60-homolog are not shown, respectively.

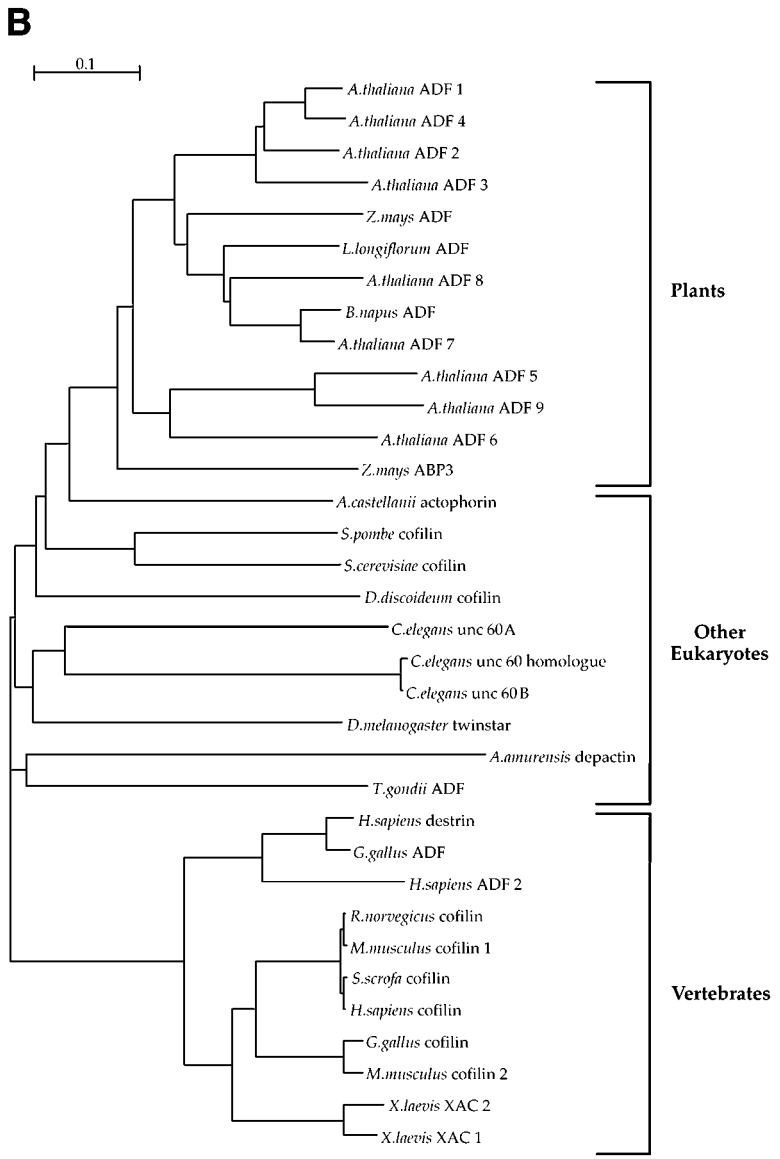

Figure 2. (Continued)

structural role. Although Ser105 and Ser106 are within hydrogen-bonding distance to backbone carbonyls of residues 101 and 102, respectively, the hydroxyl of Ser105 displays high B-factors in yeast cofilin and AtADF1, and neither of these serine hydroxyl groups is well ordered among the top 20 NMR solution structures of human destrin. Furthermore, as these serines and backbone carbonyls are all preceding the kink of helix 3, it is not clear how these hydrogen bonds would stabilize the opening of the helix between residues 104:108 and 105:109.

Conservation of Surface Character

Since the four structural representatives of the AC family have been shown to functionally interact with rabbit skeletal muscle actin in vitro, one would expect the actin-interacting regions to display some degree of similarity in surface qualities. The surface topologies of three isoform crystal structures (yeast cofilin, nonphosphorylated actophorin, and AtADF1) were compared by first superimposing the secondary structural elements and then calculating distances from the surface of one isoform to the surfaces of the other two (see Materials and Methods). On the basis of these distance calculations, it is possible to render only those surface vertices of one isoform that are within a given distance of the other two surfaces, thus visualizing those contours that are the most topologically similar. Performing this type of "surface subtraction" for the three crystal structures results in a weblike surface pattern for each isoform: the more substantial surface "patches" primarily stem from surface-exposed main-chain atoms, whereas "holes" in the surface are the result of side chains that differ in identity or rotomer conformation. Although most topologically conserved surface patches are located on turns and the edge strands of

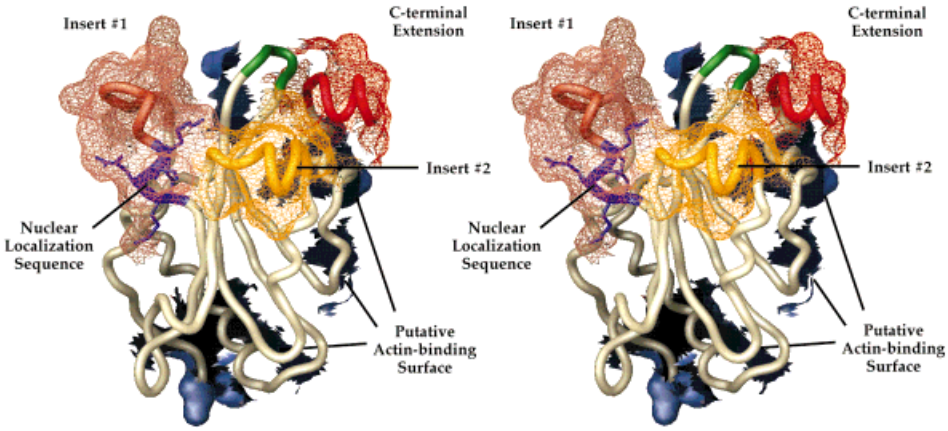

Fig. 3. A molecular surface rendering of human destrin, highlighting the vertebrate specific inserts and C-terminal extension (mesh surfaces). The loop between β-strands 4 and 5 (green) appears to be stabilized by these interactions, displaying a low to average r.m.s. deviation among the 20 top solutions, in contrast to the relatively high B-factors of the three crystal structures. Mutations that have been found to weaken or abolish actin binding are represented as a solid surface. This figure was prepared by using the program GRASP.[62]

the β-sheet, a main-chain-exposed region that lies in the middle of the putative actin-binding surface is the kink in helix 3 (Fig. 5). In addition to the exposed main-chain atoms, the topology of this region is relatively limited because of the short alanine, serine and threonine side chains at positions 104–106. These conserved features of the AC family may be critical for binding and/or depolymerization of actin filaments.

For all four isoform structures, comparisons were also made for the hydrophobic and charged surface character. The surface-exposed hydrophobic residues at position 101 and 102 were previously noted for their proximity to the two conserved actin-binding residues at positions 98 and 100 and for a possible role in protein:protein interactions.[44] We find that these residues are part of a larger, conserved hydrophobic patch, formed by Pro/Lys/Arg96, Val/Leu/Ile97, Arg/Lys98, Lys100, Met101, and Ile/Leu/Met/Val102, which covers 295 ± 35 Å^2 of solvent-exposed surface (Fig. 5). At position 96, it is interesting to note that the long aliphatic side chain of lysine or arginine found in plants maintains the hydrophobic character fulfilled by proline in nonplant isoforms.

For electrostatic surface potential, the structural representatives of the AC family exhibit one conserved and three semiconserved regions. The most electrostatically conserved region among all four structures includes a cluster of three acidic residues (93, 125, and 128) and a lysine at position 100, three of which (positions 100, 125, and 128) have been implicated in actin binding via mutagenesis (Fig. 5). Although position 125 is not negatively charged in vertebrates, the acidic character of this region is instead contributed by the side-chain carboxyl group of position 127 (destrin Asp/Glu141). The three electrostatically semiconserved regions occur at the beginning of α-helix 3 (Lys/Arg98), on the second half of α-helix 3 and β-strand 6 (Lys107, Asp108, Lys/Arg111, Lys/Arg112 and Glu/Asp120), and on α-helix 4 (position 136, primarily Glu/Asp and Lys/Arg137). Although these regions display strong sequence conservation, most side chains differ in conformation among the isoforms, resulting in locally distinct surface topologies and electrostatic distributions.

Residues implicated in actin binding (for review see Lappalainen et al [48] and Bamburg et al[49]) are generally in or proximal to highly conserved regions of the protein surface, most notably the acidic patch following β-strand 6, the hydrophobic patch at the base of α-helix 3, and the kink in the middle of α-helix 3 (Fig. 5). However, there are several instances where mutagenesis does not affect actin binding as one might expect based on the sequence conservation. Mutations of highly conserved residues that did not appear to affect actin binding include Lys107, Asp108, Lys/Arg111, and Lys/Arg112.[44] It is possible that these residues play a role in the electrostatic "steering" that has been suggested to underlie the salt-induced disruption of the AC-dependent increase in barbed-end polymerization.[7,54] Further biochemical characterization of these mutants will be required to fully understand the strong sequence conservation observed at these positions.

pH Regulation of AC Activity

As evidenced by the importance of the state of the actin-bound nucleotide, the ability of AC proteins to bind and alter actin biochemistry depends very much on physical changes in actin. The pH-dependent depolymerization shown for several AC isoforms[34,35] may be based on pH-induced structural changes in the actin filament rather than a direct effect on AC proteins themselves. Cryoelectron microscopy has recently shown that changes in pH notably alter the structure of filamentous actin, suggesting that distinct subsets of actin:actin contacts are favored at different pH values.[55] AC proteins have been shown to induce a twist in the actin filament, hypothesized to increase depolymerization by weakening actin:actin contacts.[49,50] The subsets of actin:actin filament contacts present at high pH may be more strained by the AC-induced filament twist than filament contacts at low pH. It may be a general feature of actin-binding proteins to take advantage of environmentally induced changes in the monomeric and filamentous actin structures. Crystal structure determination of the AC:actin complex will be important in furthering our understanding of this dynamic actin regulator.

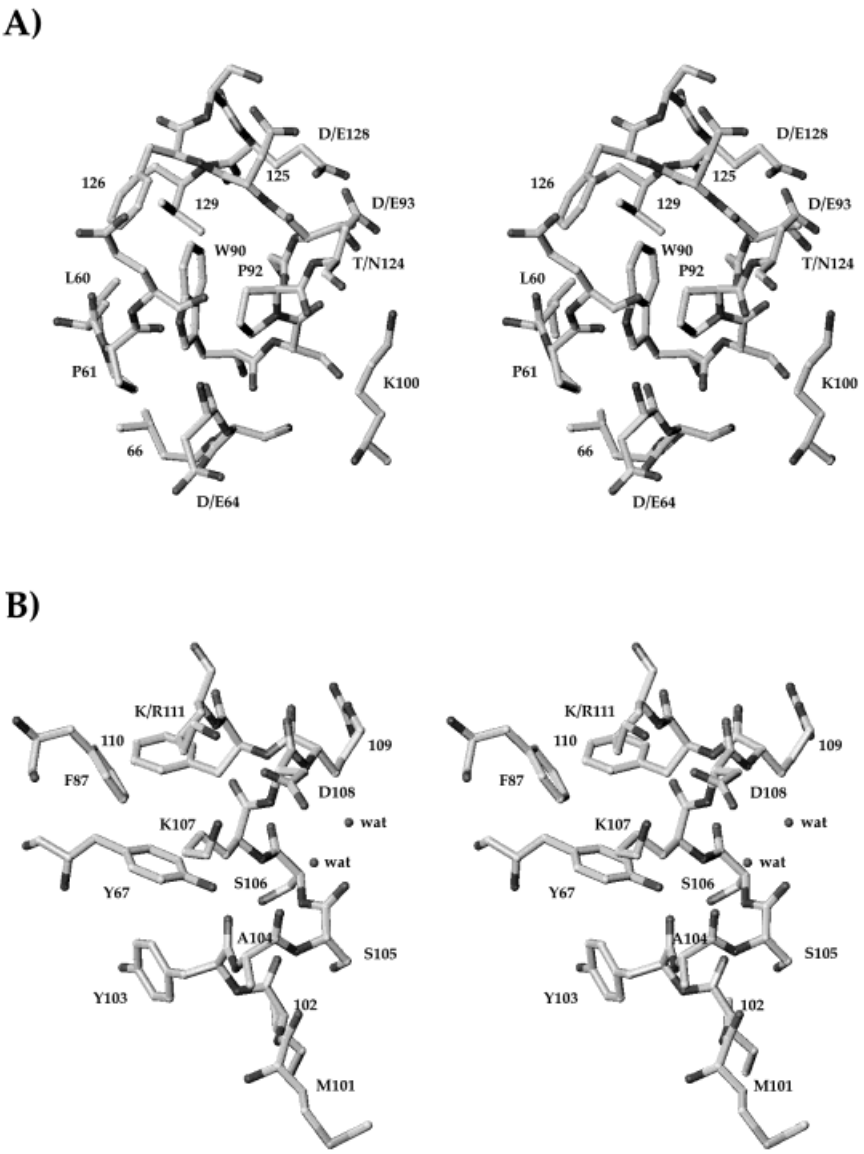

Fig. 4. **A:** Trp90 lies in the center of and interacts with a cluster of conserved residues. The tryptophan ring packs against two prolines at positions 61 and 92, a proline/aromatic typically observed at position 126, and the hydrophobic side chains of Leu60 and residue 129. A single hydrogen bond between the indole ring and the backbone carbonyl of residue 61 is conserved in all structures. These interactions constrain the positioning of the loops preceding helices 3, 4, and β-strand 4 from which the conserved residues 64–66, Lys100, and the acidic residues at positions 93, 123, and 126 project. Note that the yeast cofilin leucine replaces the conventional AC arginine at position 66, losing the conserved electrostatic interaction with Asp/Glu64 but maintaining the hydrophobic character. This figure was prepared by using the program O[59] and the coordinates of yeast cofilin.[30] **B:** Stabilizing interactions in and around the kink in α-helix 3. Bending of the α-helix about residue 106 disrupts the α-helical hydrogen bonding pattern between the carbonyl:amide pairs 104:108 and 105:109. The hydroxyl group of Tyr103 makes a hydrogen bond to the backbone amide of residue 34 (not shown), whereas the hydroxyl of Tyr67 hydrogen bonds to the backbone carbonyl of residue 103. Mutagenesis of either of these tyrosines to phenylalanine disrupts or weakens actin binding, emphasizing the structural importance of this region.[21,45] In the crystal structures of AtADF1 and the phosphorylated form of actophorin, two water molecules were observed at the kink, each making hydrogen bonds to otherwise unsatisfied carbonyl and amide backbone atoms. This figure was prepared by using the program O[59] and the coordinates of AtADF1.

MATERIALS AND METHODS

Purification

AtADF1 was purified as previously described[7] with some modifications. Briefly, *E. coli* strain BL21(DE3) transformed with pET16b carrying AtADF1 was induced with 0.5 mM of IPTG at 37°C and harvested after 3 h. Cell pellets were stored at −80°C until needed. AtADF1 was extracted from cell pellets by using the freeze-thaw technique.[56] After resuspension in 10 mM of Tris-HCl, pH 8.2, 50 mM of NaCl, 0.1 mM of PMSF and 5 mM of DTT (DEAE buffer), slurry was clarified by centrifugation at 3K RPM for 20 min, 39K RPM for 1h, and then applied to a DEAE-Fast Flow column (Pharmacia) equilibrated in DEAE buffer. Flow-through fractions containing AtADF1 were then applied to an SP-Fast Flow column (Pharmacia) equilibrated in 10 mM of PIPES, pH 6.2, 25 mM of NaCl, 5 mM of DTT, and eluted with a NaCl gradient (75–425mM). Fractions containing pure AtADF1 were dialyzed against 10 mM of KPO_4, pH 7.6, 1 mM of DTT, and concentrated to 18–25mg/mL for crystallization.

Crystallization and Data Collection

Crystals grew in hanging drops at 4°C, over a well solution of 1.6 M $(NH_4)_2SO_4$, 100 mM of citrate, pH 5.8, in drops of 5 μL of well solution, 4 μL of protein, and 1 μL of 20mM LDAO (CalBiochem). Crystals appeared after 3–4 days and reached approximately 1.0 mm × 0.5 mm × 0.15 mm after 21 days. Diffraction data were collected on a single crystal at 100K using a Rigaku RU-H2R rotating copper anode and an RAXIS II-C detector, and processed with DENZO and SCALEPACK.[57] Crystal parameters and data collection statistics are given in Table I.

Model Building and Refinement

Molecular replacement was performed by using the program AMoRe.[58] The structure of yeast cofilin was used

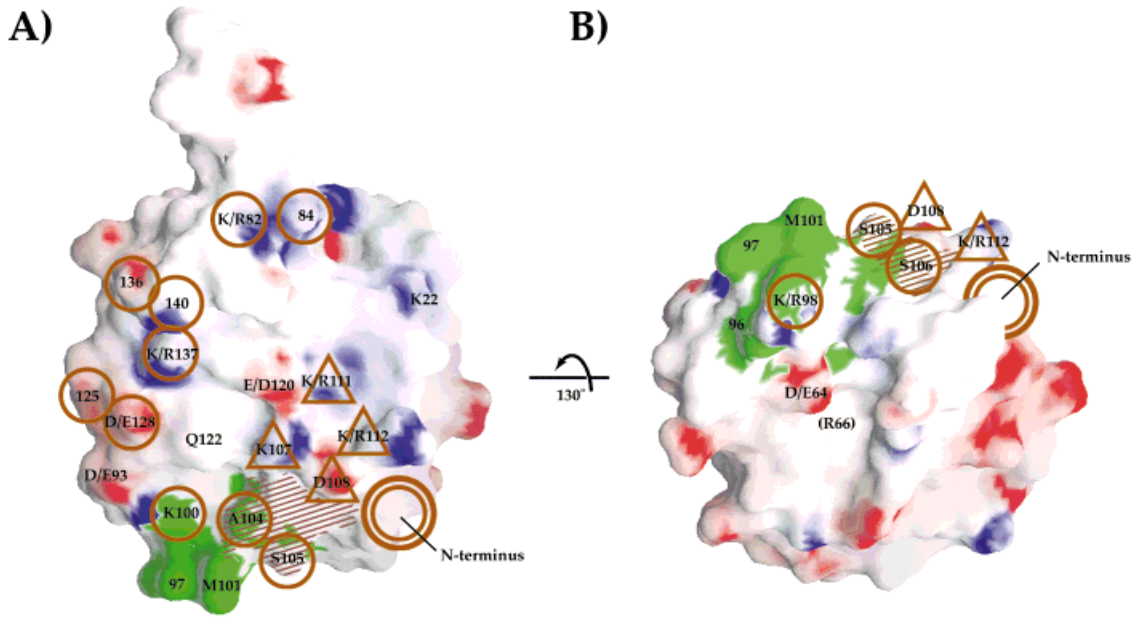

Fig. 5. **A,B:** An overview of the surface character. Blue and red represent the positive and negative electrostatic surface potential of yeast cofilin[30] calculated by using the program GRASP.[62] Encircled residues have been shown to reduce or abolish actin binding, whereas residues enclosed with triangles have little effect on binding despite high sequence conservation.[21,43–46] The first five residues of the N-terminus are disordered in the crystal structure (double circle), though their presence is required for actin binding. The hatched surface represents a topologically conserved surface patch in and around the kink of α-helix 3. The green surface represents a conserved, surface exposed hydrophobic patch contributed by residues 96–98 and 100–102. As in Figure 4, the residue at position 66 is arginine in most AC family members (leucine in yeast cofilin) and displays electrostatic interactions with Asp/Glu64 in other family members. The orientation in (A) is similar to that of Figure 1. Rotation of (A) by 130° about the x-axis yields the orientation in (B).

as the search model (pdb accession code:1COF) with all nonconserved side chains substituted with alanine. This model yielded a crystallographic dimer with an extended β-sheet shared by two monomers. The helical C-terminus of cofilin produced serious steric clashes at the crystallographic dimer interface. No density was observed for the C-terminal 15 residues, and this region was removed from the model in the first building cycle. Although helical density corresponding to the C-terminus did not appear in the building process, a single tube of density near the C-terminus was consistently observed throughout building and refinement. After most of the AtADF1 side chains were built, the persisting tube of density was identified as lauryldimethylamine oxide (LDAO) on the basis of size, shape, and chemical environment. Building was performed by using the program O.[59] The refinement process began with X-PLOR[60] and used CNS[61] in the final stages. In the final model, the first 4 and last 11 residues were omitted.

Structural Analysis

The pdb accession codes for the structures used in this analysis are 1AK6/1AK7 (human destrin[47]), 1COF (yeast cofilin[30]), 1AHQ (*Acanthamoeba* actophorin[31]), 1CNU (phosphorylated actophorin[32]) and 1F7S (*Arabidopsis* ADF1, this study). Superpositions and r.m.s.d. calculations were performed by using the program O.[59] For analysis of surface topologies, the program GRASP[62] was used to first generate molecular surfaces of the three nonvertebrate crystal structures (yeast cofilin, nonphosphorylated actophorin and AtADF1). With the three nonvertebrate structures superimposed, the distances were calculated between each pair of surfaces. This calculation assigned a minimum distance to each surface vertex corresponding to the nearest surface vertex on the other two surfaces. With the arbitrary cutoff of 1.0 Å, it was possible to display only those surface vertices that were $<$1.0Å from the other two surfaces. As stated in the text, the most topologically conserved surface patches remaining after this procedure were essentially surface exposed main-chain and C_β atoms.

Coordinates

The coordinates and experimental amplitudes have been deposited in the Protein Data Bank (PDB accession code: 1F7S).

ACKNOWLEDGMENTS

We thank Kevin Parris, Ron Shigeta, Yigong Shi, and Kurt Thorn for crystallographic discussions and advice. We also thank Herwig Schüler for helpful suggestions on the manuscript. This work was also supported by grants from the National Institutes Health (GM-07312 for G.D.B. and GM-44038 for C.E.S.) and an NIH predoctoral training grant in molecular biophysics (GM08309 for I.M.N.).

REFERENCES

1. Mellström K, Höglund A-S, Nistér M, Heldin C-H, Westermark B, Lindberg U. The effect of platelet-derived growth factor on morphology and motility of human glial cells. J Muscle Res Cell Motil 1983;4:589–609.
2. Perrin D, Möller K, Hanke K, Söling H-D. cAMP and Ca^{2+}-mediated secretion in parotid acinar cells is associated with reversible changes in the organization of the cytoskeleton. J Cell Biol 1992;116:127–134.
3. Sanger JM, Mittal B, Dome JS, Sanger JW. Analysis of cell division using fluorescently labeled actin and myosin in living PtK2 cells. Cell Motil Cytoskeleton 1989;14:201–219.
4. Moon A, Drubin DG. The ADF/cofilin proteins: stimulus-responsive modulators of actin dynamics. Mol Biol Cell 1995;6:1423–1431.
5. Chen H, Bernstein BW, Bamburg JR. Regulating actin-filament dynamics in vivo. Trends Biochem Sci 2000;25:19–23.
6. Rosenblatt J, Agnew BJ, Abe H, Bainburg JR, Mitchison TJ. *Xenopus* actin depolymerizing factor/cofilin (XAC) is responsible for the turnover of actin filaments in *Listeria monocytogenes* tails. J Cell Biol 1997;136:1323–1332.
7. Carlier M-F, Laurent V, Santolini J, et al. Actin depolymerizing factor (ADF/Cofilin) enhances the rate of filament turnover: implication in actin-based motility. J Cell Biol 1997;136:1307–1323.
8. Lappalainen P, Drubin DG. Cofilin promotes rapid actin filament turnover in vivo. Nature 1997;388:78–82.
9. Moon AL, Janmey PA, Louie KA, Drubin DG. Cofilin is an essential component of the yeast cortical cytoskeleton. J Cell Biol 1993;6:1423–1431.
10. Iida K, Moriyama K, Matsumoto S, Kawasaki H, Nishida E, Yahara I. Isolation of a yeast essential gene, COF1, that encodes a homologue of mammalian cofilin, a low-Mr actin-binding and depolymerizing protein. Gene 1993;124:115–120.
11. McKim KS, Matheson C, Marra MA, Wakarchuk MF, Bailie DL. The *Caenorhabditis elegans* unc-60 gene encodes protein homologous to a family of actin-binding proteins. Mol Gen Genet 1994;242:346–357.
12. Gunsalus KC, Bonaccorsi S, Williams E, Verni F, Gatti M, Goldberg ML. Mutations in twinstar, a *Drosophila* gene encoding a cofilin-ADF homologue, result in defects in centrosome migration and cytokinesis. J Cell Biol 1995;131:1243–1259.
13. Bamburg JR, Harris HE, Weeds AG. Partial purification and characterization of an actin depolymerizing factor from brain. FEBS Lett 1980;121:187–182.
14. Nishida E, Maekawa S, Muneyuki E, Sakai H. Actin of a 19K protein from porcine brain on actin polymerization: a new functional class of actin-binding proteins. J Biochem 1984;95:387–398.
15. Mabuchi I. Effects of muscle proteins on the interaction between actin and an actin-depolymerizing protein from starfish oocytes. J Biochem (Tokyo) 1982;92:1439–1447.
16. Cooper JA, Blum JD, Williams RC, Pollard TD. Purification and characterization of actophorin, a new 15,000-dalton actin binding protein from *Acanthamoeba castellanii*. J Biol Chem 1986;261:477–485.
17. Maciver SK, Zot HG, Pollard TD. Characterization of actin filament severing by actophorin from *Acanthamoeba castellanii*. J Cell Biol 1991;115:1611–1620.
18. Hayden SM, Miller PS, Brauweiler A, Bamburg JR. Analysis of the interactions of actin depolymerizing factor with G- and F-actin. Biochemistry 1993;32:9994–10004.
19. Carlier MF, Ressad F, Pantaloni D. Control of actin dynamics in cell motility: role of ADF/cofilin. J Biol Chem 1999;274:33827–33830.
20. Theriot JA. Accelerating on a treadmill: ADF/cofilin promotes rapid actin filament turnover in the dynamic cytoskeleton. J Cell Biol 1997;136:1165–1168.
21. Moriyama K, Yahara I. Two activities of cofilin, severing and accelerating directional depolymerization of actin filaments, are affected differentially by mutations around the actin-binding helix. EMBO J 1999;18:6752–6761.
22. Du J, Frieden C. Kinetic studies on the effect of yeast cofilin on yeast actin polymerization. Biochemistry 1998;37:13276–13284.
23. Blanchoin L, Pollard TD. Interaction of actin monomers with *Acanthamoeba* actophorin (ADF/cofilin) and profilin. J Biol Chem 1998;273:25106–25111.
24. Maciver SK, Pope BJ, Whytock S, Weeds AG. The effect of two actin depolymerizing factors (ADF/cofilins) on actin filament turnover: pH sensitivity of F-actin binding by human ADF, but not of *Acanthamoeba* actophorin. Eur J Biochem 1998;256:388–397.
25. Ichetovkin I, Han J, Pang KM, Knecht DA, Condeelis JS. Actin filaments are severed by both native and recombinant *Dictyostelium* cofilin but to different extents. Cell Motil Cytoskeleton 2000;45:293–306.
26. Arber S, Barbayannis FA, Hanser H, et al. Regulation of actin dynamics through phosphorylation of cofilin by LIM-kinase. Nature 1998;393:805–809.
27. Yang N, Higuchi O, Ohashi K, et al. Cofilin phosphorylation by LIM-kinase 1 and its role in Rac-mediated actin reorganization. Nature 1998;393:809–812.
28. Morgan TE, Lockerbie RO, Minamide LS, Browning MD, Bamburg JR. Isolation and characterization of a regulated form of actin depolymerizing factor. J Cell Biol 1993;122:623–633.
29. Agnew BJ, Minamide LS, Bamburg JR. Reactivation of phosphorylated actin depolymerizing factor and identification of the regulatory site. J Biol Chem 1995;270:17582–17587.
30. Fedorov AA, Lappalainen P, Fedorov EV, Drubin DG, Almo SC. Structure determination of yeast cofilin. Nat Struct Biol 1997;4:366–369.
31. Leonard SA, Gittis AG, Petrella EC, Pollard TD, Lattman EE. Crystal structure of the actin-binding protein actophorin from Acanthamoeba. Nat Struct Biol 1997;4:369–373.
32. Blanchoin L, Robinson RC, Choe S, Pollard TD. Phosphorylation of *Acanthamoeba* actophorin (ADF/cofilin) blocks interaction with actin without a change in atomic structure. J Mol Biol 2000;295:203–211.
33. Yonezawa N, Homma Y, Yahara I, Sakai H, Nishida E. A short sequence responsible for both phosphoinositide binding and actin binding activities of cofilin. J Biol Chem 1991;266:17218–17221.
34. Yonezawa N, Nishida E, Sakai H. pH control of actin polymerization by cofilin. J Biol Chem 1985;260:14410–14412.
35. Hawkins M, Pope B, Maciver SK, Weeds AG. Human actin depolymerizing factor mediates a pH-sensitive destruction of actin filaments. Biochemistry 1993;32:9985–9993.
36. Ingber DE, Prusty D, Frangioni JV, Cragoe EJ, Lechene C, Schwartz MA. Control of intracelluar pH and growth by fibronectin in capillary endothelial cells. J Cell Biol 1990;110:1803–1811.
37. Schwartz MA, Ingber DE, Lawrence M, Springer TA, Lechene C. Multiple integrins share the ability to induce elevation of intracellular pH. Exp Cell Res 1991;195:533–535.
38. Moolenaar WH, Tsien RY, van der Saag PT, de Laat SW. Na^+/H^+ exchange and cytoplasmic pH in the action of growth factors in human fibroblasts. Nature 1983;304:645–648.
39. Paris S, Pouyssegur J. Growth factors activate the Na^+/H^+ antiporter in quiescent fibroblasts by increasing its affinity for intracellular H^+. J Biol Chem 1984;259:10989–10994.
40. Maciver SK, Weeds AG. Actophorin preferentially binds monomeric ADP-actin over ATP-actin: consequences for cell locomotion. FEBS Lett 1994;347:251–256.
41. Ressad F, Didry D, Xia GX, et al. Kinetic analysis of the interaction of actin-depolymerizing factor (ADF)/cofilin with G- and F-actins. Comparison of plant and human ADFs and effect of phosphorylation. J Biol Chem 1998;273:20894–20902.
42. Nishida E, Iida K, Yonezawa N, Koyasu S, Yahara I, Sakai H. Cofilin is a component of intranuclear and cytoplasmic actin rods induced in cultured cells. Proc Natl Acad Sci USA 1987;84:5262–5266.
43. Moriyama K, Yonezawa N, Sakai H, Yahara I, Nishida E. Mutational analysis of an actin-binding site of cofilin and characterization of chimeric proteins between cofilin and destrin. J Biol Chem 1992;267:7240–7244.
44. Lappalainen P, Fedorov EV, Fedorov AA, Almo SC, Drubin DG. Essential functions and actin-binding surfaces of yeast cofilin revealed by systematic mutagenesis. EMBO J 1997;16:5520–5530.
45. Jiang CJ, Weeds AG, Khan S, Hussey PJ. F-actin and G-actin binding are uncoupled by mutation of conserved tyrosine residues in maize actin depolymerizing factor (ZmADF). Proc Natl Acad Sci USA 1997;94:9973–9978.
46. Ono S, Baillie DL, Benian GM. UNC-60B, an ADF/cofilin family protein, is required for proper assembly of actin into myofibrils in *Caenorhabditis elegans* body wall muscle. J Cell Biol 1999;145:491–502.

47. Hatanaka H, Ogura K, Moriyama K, Ichikawa S, Yahara I, Inagaki F. Tertiary structure of destrin and structural similarity between two actin-regulating protein families. Cell 1996;85:1047–1055.
48. Lappalainen P, Kessels MM, Cope MJ, Drubin DG. The ADF homology (ADF-H) domain: a highly exploited actin-binding module. Mol Biol Cell 1998;9:1951–1959.
49. Bamburg JR, McGough A, Ono S. Putting a new twist on actin: ADF/cofilins modulate actin dynamics. Trends Cell Biol 1999;9:364–370.
50. McGough A, Pope B, Chiu W, Weeds A. Cofilin changes the twist of F-actin: implications for actin filament dynamics and cellular function. J Cell Biol 1997;138:771–781.
51. Matsuzaki F, Matsumoto S, Yahara I, Yonezawa N, Nishida E, Sakai H. Cloning and characterization of porcine brain cofilin cDNA: cofilin contains the nuclear transport signal sequence. J Biol Chem 1988;263:11564–11568.
52. Abe H, Nagaoka R, Obinata T. Cytoplasmic localization and nuclear transport of cofilin in cultured myotubes. Exp Cell Res 1993;206:1–10.
53. Conti E, Uy M, Leighton L, Blobel G, Kuriyan J. Crystallographic analysis of the recognition of a nuclear localization signal by the nuclear import factor karyopherin alpha. Cell 1998;94:193–204.
54. Sept D, Elcock AE, McCammon JA. Computer simulations of actin polymerization can explain the barbed-pointed end asymmetry. J Mol Biol 1999;294:1181–1189.
55. Lukoyanova N, Orlova A, Egelman E. Structural polymorphism in F-actin: modification of F-actin structure by pH, temperature, ionic strength, and labeling of C-terminus. New Orleans, Louisiana: Biophysical Society 44th Annual Meeting 2000.
56. Johnson BH, Hecht MH. Recombinant proteins can be isolated from *E. coli* cells by repeated cycles of freezing and thawing. Biotechnology 1994;12:1357–1360.
57. Otwinowski Z. Oscillation data reduction program. In: Sawyer L, Isaacs N, Bailey S, editors. Proceedings of the CCP4 Study Weekend: Data Collection and Processing. Warrington, UK: SERC Daresbury Laboratory; 1993. p 56–62.
58. Navaza J. AMoRe: an automated package for molecular replacement. Acta Crystallogr 1994;A50:157–167.
59. Jones TA, Zou J-Y, Cowtan SW, Kjeldgaard M. Improved methods for building protein models in electron density maps and the location of errors in these models. Acta Crystallogr 1991;A47:110–119.
60. Brünger AT. XPLOR Version 3.1. A System for X-ray Crystallography and NMR.New Haven, CT: Yale University Press, 1993.
61. Brünger AT, Adams PD, Clore GM, et al. Crystallography & NMR system (CNS): a new software system for macromolecular structure determination. Acta Crystallogr D 1998;54:905–921.
62. Nicholls A. GRASP: Graphical Representation and Analysis of Surface Properties. New York: Columbia University, 1993.
63. Frishman D, Argos P. Knowledge-based protein secondary structure assignment. Proteins 1995;23:566–579.
64. Barton GJ, Sternberg MJ. Flexible protein sequence patterns: a sensitive method to detect weak structural similarities. J Mol Biol 1990;212:389–402.
65. Barton GJ. An efficient algorithm to locate all locally optimal alignments between two sequences allowing for gaps. Comput Appl Biosci 1993;9:729–734.
66. Thompson JD, Higgins DG, Gibson TJ. CLUSTAL W: improving the sensitivity of progressive multiple alignment through sequence weighting, position-specific gap penalties and weight matrix choice. Nucleic Acids Res 1994;22:4673–4680.
67. Perriere G, Gouy M. WWW-Query: an on-line retrieval system for biological sequence banks. Biochemie 1996;78:364–369.